

Charge-parity symmetry observed through Friedel oscillations in chiral charge-density wavesJ. Ishioka,¹ T. Fujii,² K. Katono,¹ K. Ichimura,^{1,3} T. Kurosawa,⁴ M. Oda,^{3,4} and S. Tanda^{1,3,*}¹*Department of Applied Physics, Hokkaido University, Sapporo 060-8628, Japan*²*Department of Physics, Asahikawa Medical College, Asahikawa 078-8510, Japan*³*Center of Education and Research for Topological Science and Technology, Hokkaido University, Sapporo 060-8628, Japan*⁴*Department of Physics, Hokkaido University, Sapporo 060-0810, Japan*

(Received 21 July 2011; revised manuscript received 21 November 2011; published 27 December 2011)

We discovered a chiral behavior of Friedel oscillations (FOs), which have both triangular symmetry and inverse chirality from chiral charge-density waves (CDWs) in 1T-TiSe₂ by using scanning tunneling microscopy (STM). Surprisingly, the existence of FOs with the opposite chirality to the underlying CDWs suggests that the excess electron induced by impurity reduces the local helicity of CDWs without CDW breaking. This FOs can be explained with a two-branch model with different chiralities, which permits excitation from one branch to another, that is, Dirac-type dispersion. Moreover, we found two states that correspond to electron addition and electron removal. In terms of the chirality of electrons, these two states are the same. This result provides an evidence for the charge-parity (CP) symmetry conservation in CDW systems.

DOI: [10.1103/PhysRevB.84.245125](https://doi.org/10.1103/PhysRevB.84.245125)

PACS number(s): 71.45.Lr, 68.37.Ef, 72.80.Ga, 73.22.Gk

I. INTRODUCTION

In nature, there are parity violations with several different scales. For example, in particle physics, parity symmetry is broken in the β decay of ⁶⁰Co.¹ DNA mainly has a right-handed double-helix structure.² In liquid crystal, the molecules are arranged with helical stacking in the cholesteric phase.³ Recently, it has been reported that a chiral p -wave superconductor breaks parity symmetry.⁴ Thus, the macroscopic quantum order in materials can also break mirror symmetry. Using a macroscopic quantum system, we have now reached the stage of being able to approach the issue of the asymmetric property of the universe.

We have discovered chiral charge-density waves (CDWs) in 1T-TiSe₂,⁵ in which the macroscopic quantum state exhibits helicity in a static structure. If a charged impurity is added to an electron system, the Friedel oscillation for screening is induced.⁶⁻⁸ Does the FO in a chiral CDW have helicity? If so what is the relationship between the FO and underlying CDWs? In systems composed of atoms or molecules, it is difficult for the antihelix of the system to emerge spontaneously once the helicity of the entire system has been fixed. Moreover, a change in the number of components will not affect the overall helicity. However, this argument does not necessarily hold for a macroscopic quantum system. A CDW system is the most promising system for realizing the direct and local observability of the interaction between a macroscopic quantum state and the electronic perturbation caused by impurities.

In this study, we discovered a “triangular” FO attributed to the chiral CDWs of TiSe₂. By using an *in situ* cleavage method in an ultra-high vacuum STM chamber, we found that triangular FOs have chirality based on the intensity of the tunnel current. Unexpectedly, the observed Friedel oscillations have inverse chirality from underlying CDWs. To develop locally inverted helicity, electron systems need internal right-handed and left-handed states. That is, our results strongly suggest that the CDWs in 1T-TiSe₂ are Dirac-type CDWs composed of right- and left-handed components. Essentially, the electron system conserves parity symmetry,

however CDW excitation breaks the parity symmetry. Our discovery of a Dirac-type CDW provides another approach for investigating Dirac fermions. The charge-parity (CP) symmetry conservation in CDW systems is revealed by FO.

1T-TiSe₂⁹⁻¹⁹ crystallizes in a 1T-CdI₂ type structure. The crystal is constructed of Se-Ti-Se layers. These Se-Ti-Se layers consist of a plane occupied by Ti atoms that is sandwiched between similar planes of Se atoms on either side. All the Se-Ti-Se layers are weakly accumulated by the van der Waals attraction along the c axis. 1T-TiSe₂ undergoes a CDW transition into a $2a_0 \times 2a_0 \times 2c_0$ superlattice ($a_0 = 3.54$ Å, $c_0 = 6.00$ Å are lattice constants) at $T_c = 200$ K.^{9,10}

II. EXPERIMENTAL

We synthesized a single crystal of 1T-TiSe₂ with Ti self-intercalation at 800 °C, and the STM images were obtained as in Ref. 5. By *in situ* cleavage method in the specimen chamber at 77 K and 10^{-8} Pa, we obtained an atomically defect-free Se surface.

III. RESULTS AND DISCUSSION

Figure 1(a) shows a tunneling current image of the Se surface of TiSe₂. We observed chiral CDWs as reported in our previous paper.⁵ We found triangular FOs as denoted by the white and black solid circles [Fig. 1(a)]. The brightness corresponds to the intensity of the tunneling current. The bright point corresponds to Se atoms, which form triangular lattices with a lattice constant a_0 . We confirmed that a $2a_0 \times 2a_0$ charge modulation develops in the dark region enclosed with a rectangle [Fig. 1(a)]. We found clearly triangular charge localizations with the same orientation. On the assumption that this charge localization is formed by the three planar waves, each component of the planar waves oscillates spatially with a wavelength $2a_0$ and maximum decay length of 1 nm. This wavelength is equal to the planar components of the CDW \mathbf{q} vectors in TiSe₂, and the decay length is comparable to the Thomas-Fermi screening length. Therefore this is consistent with a FO in terms of these characteristic lengths.^{20,21}

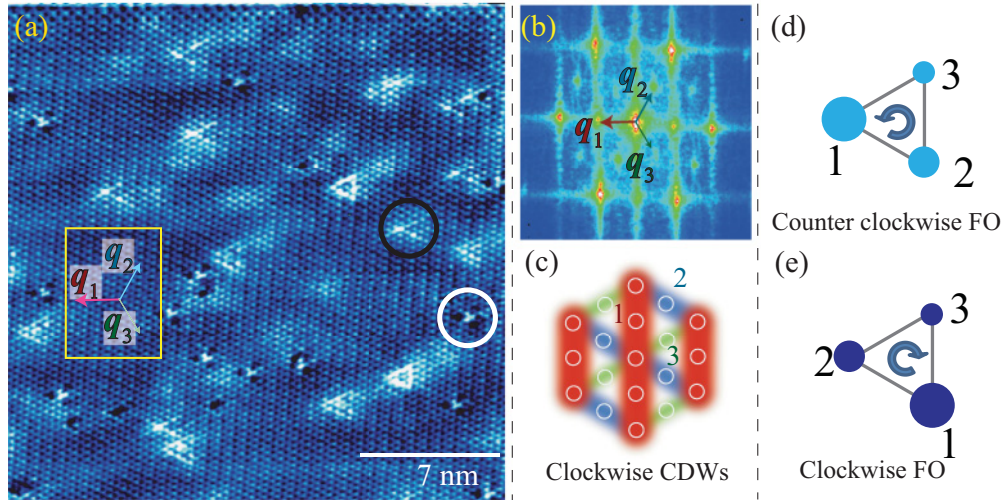


FIG. 1. (Color online) (a) 20 nm \times 20 nm STM image measured at $V_s = 180$ mV and $I_t = 0.2$ nA at $T = 84$ K, (b) Fourier transformation of dark areas in (a), (c) interpretation of underlying CDW distribution in real space, and (d),(e) schematic images of bright FO and dark FO, respectively.

We analyzed the underlying CDWs using a Fourier transformation (FT). Figure 1(b) shows a FT image of the dark area shown by the area outlined with a rectangle in Fig. 1(a). The background chiral CDW shows the clockwise phase.⁵ The interpretation of the FT image in real space is shown in Fig. 1(c). The charge concentration is indicated by the deeply colored part. Each color corresponds to the CDW components. The difference between the three CDW amplitudes causes chirality. Fourier analysis corresponds to real space analysis. As indicated by the black and white circles in Fig. 1(a), we found two types of triangular FOs, that were reproducible. And we found an intensity difference for each atom as shown schematically in Figs. 1(d) and 1(e). To investigate the chirality in FOs, we analyzed the intensity of the charge on each atom.

Figures 2(a) and 2(b) show bright FO and dark FOs indicated in yellow circles. We integrated the tunneling current in Figs. 2(a) and 2(b). Then, we averaged the intensity ratios of the three sites for the observed FOs. In Fig. 2(a), the intensity ratio of the triad peaks is $1 \pm 0.22 : 0.53 \pm 0.08 : 0.40 \pm 0.07$. We defined the chirality of the bright FOs based on their height from the background level. The chirality is anticlockwise. We defined the chirality of the dark FOs based on their depth from the background level. The average intensity on clockwise dark FOs and anticlockwise dark FOs are $1 \pm 0.12 : 0.75 \pm 0.10 : 0.49 \pm 0.16$ and $1 \pm 0.11 : 0.87 \pm 0.08 : 0.63 \pm 0.08$, respectively. From those results, a number-weighted mean ratio in dark FOs is $1 \pm 0.12 : 0.80 \pm 0.09 : 0.55 \pm 0.13$. The chirality is clockwise. In summary, bright FOs are anticlockwise and dark FOs are clockwise, as shown in Fig. 2. It must be emphasized that if the bright FOs and dark FOs are superimposed, a constant charge density cannot occur because of the opposite chirality of those FOs.

We performed the same analysis on anticlockwise CDWs [Figs. 2(c) and 2(d)]. The results are listed in Table I with the results of Fig. 1. With anticlockwise CDWs, we confirmed the tendency for bright FOs to be clockwise and for dark FOs to

be anticlockwise [Figs. 2(c) and 2(d)]. Therefore, there is a relationship whereby the chirality of bright FOs is opposite to that of the underlying CDWs and that of dark FOs is the same as that of the CDWs.

To understand the origin of the triangular FOs, we compared them with results for FOs in CDW material, TaS₂ and TaSe₂.⁸ FOs were observed with hexagonal or spherical symmetry attributed to the two-dimensional CDWs. On the other hand,

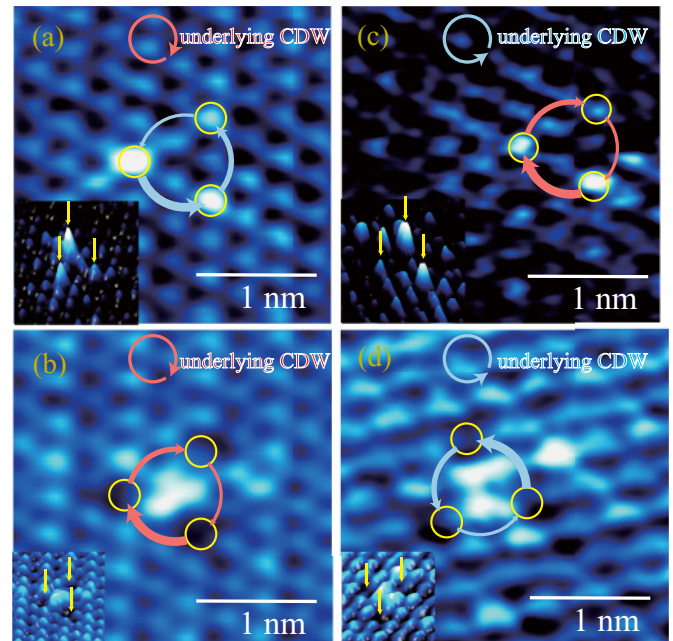


FIG. 2. (Color online) Friedel oscillations in clockwise CDW [(a),(b)] and anticlockwise CDW [(c),(d)]. STM images of (c) $V_s = 180$ mV and $I_t = 0.35$ nA at $T = 84$ K and (d) $V_s = 800$ mV and $I_t = 0.40$ nA at $T = 6.3$ K. Three-dimensional plots are inset in each image, and each peak and gap is indicated by yellow arrows. The red and blue arrows indicate clockwise and anticlockwise CDWs and FOs, respectively.

TABLE I. Statistical analysis for chirality of FOs in clockwise and anticlockwise CDWs. We calculated the “averaged” intensity after sorting them in descending order of the value. With a dark FO, we averaged the intensity with weight ratio based on the number of clockwise and anticlockwise FOs.

Underlying CDWs				
Type of FO				
Sample Number (clockwise:anti-clockwise)	7 (0 : 7)	11 (7 : 4)	1 (1 : 0)	3 (0 : 3)
Average intensity of FOs	1 ± 0.22 : 0.53 ± 0.08 : 0.40 ± 0.07	1 ± 0.12 : 0.80 ± 0.09 : 0.55 ± 0.13	1 : 0.73 : 0.38	1 ± 0.34 : 0.67 ± 0.30 : 0.45 ± 0.27
Chirality of FOs				

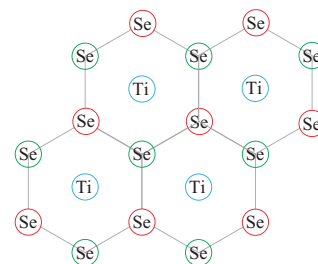
our results show a triangular symmetry structure. What is the difference between TaS₂ and TiSe₂? We focused on the phase pinning of CDWs on Friedel oscillation. As regards screening the impurities in CDW systems, the static energy is smaller when the fixing CDW phase and the phase of the FOs are fixed. When phase pinning occurs with the three components in a two-dimensional CDW, hexagonal charge localization from an impurity center will be induced. This picture corresponds to the FOs observed in TaS₂. On the other hand, in TiSe₂, the c^* vectors (* indicates a reciprocal vector) means that FOs include c -axis components.¹² Basically, a chiral CDW is a state with three CDW components with different wave function phases. When the three CDW components have different phases, the wavefront is not fixed at the point. Therefore the FOs do not form a hexagon, and it would be more proper to think triangular charge localizations are contributed from collective electronic states of 1T-TiSe₂.

Recently, an explanation for triangular charge localizations has been attempted from the viewpoint of crystallographic structure. STM measurements on 1T-TiSe₂ at room temperature was performed by A. S. Razinkin *et al.*, and the authors also found triangular charge localizations similar to our results.²² A. S. Razinkin *et al.* had discussed that a triangular charge localization is attributed to some defects which change the local crystallographic structure from 1T (octahedral coordination for Ti) to 2H (prismatic coordination for Ti). However, this model does not seem to cover the cases of either 1T-TaS₂ or 1T-TaSe₂,⁸ systems which have the same coordination for metal atoms. Moreover, we found that in magnetic field at low temperature, those FOs are enhanced. That effect cannot be explained within crystallographic structure change, and the magnetic field effect will be reported elsewhere. It is more appropriate to think that triangular charge localizations are mainly contributed from collective electronic states of 1T-TiSe₂ rather than to think that result from some crystallographic bonding reconstruction related to Frenkel defects.²³

For further understanding, we discuss why the chirality of the FOs is the inverse of that of the underlying CDWs. Chiral inversion needs a mirror plane, but once chiral charge density waves are excited, all of the mirror planes disappear. One

possible reason is that the local mirror inversion is induced by Ti atoms. We focused on the crystallographic structure with 1T-TiSe₂ with the self-intercalation of Ti in the van der Waals gap. Figure 3 shows the arrangement of each atom in the Se-Ti-Se lattice. 1T-TiSe₂ is composed of a triangular lattice of Se and Ti. The unit sheets of Se-Ti-Se repeat along the c axis in an ordinary sequence. For excess atoms, a site immediately above the Ti atoms is fitted to intercalate in the van der Waals gap because of the neighboring Se lattices. An intercalated Ti atom induces a set of mirror planes for space inversion along the z axis (Fig. 3). If a chiral field is attached in the entire space, the added atom plays a role in the chiral inversion. On the other hand, the removal of an atom from the original layer does not make a mirror plane. The inversion of chirality at an

(a) Top view



(b) Side view

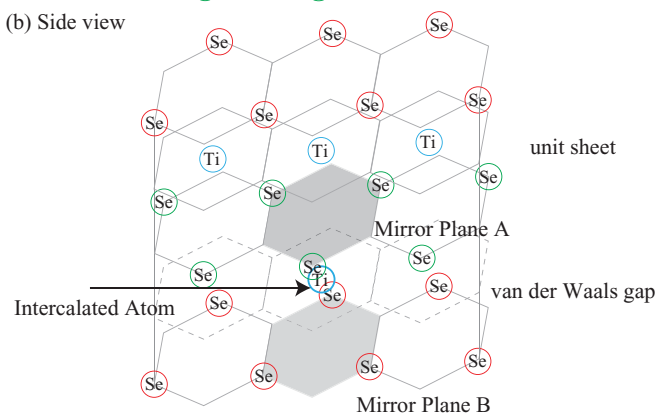


FIG. 3. (Color online) (a) Top view and (b) side view of crystallographic structure of 1T-TiSe₂ with self-intercalated Ti atom.

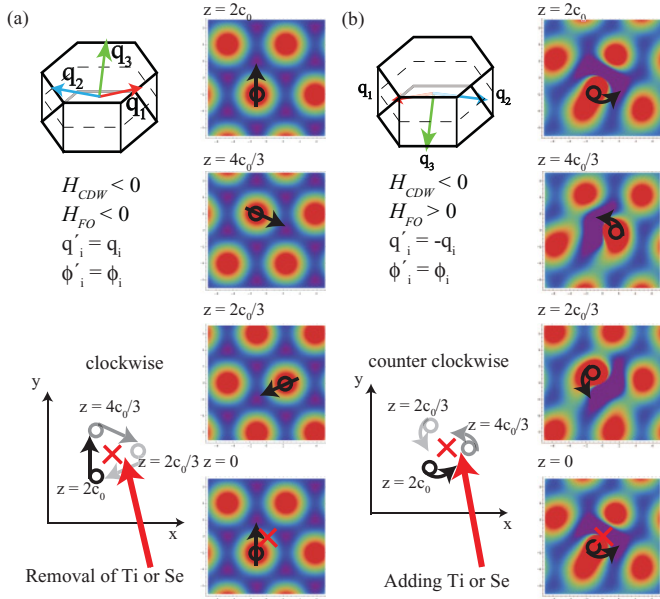


FIG. 4. (Color online) Schematic representation of chirality at Friedel oscillation around (a) vacancy of Se and (b) intercalation of Ti atom.

FO can be understood by the inversion of each wave vector at an impurity.

To illustrate qualitatively that a local mirror plane induces inversed chirality around an FO, we performed a numerical calculation of the electronic distribution by the simplest model considering planer waves of either CDWs or screening electron. Figure 4 shows a numerical calculation of the summation of three CDW components. This image shows electronic distribution as a function of x, y ,

$$\rho_{CDW}(\mathbf{r}) = \sum_{i=1,2,3} \cos(\mathbf{q}_i \cdot \mathbf{r} + \phi_i), \quad (1)$$

where $\mathbf{q}_1 = 1/2\mathbf{a}^* + 1/2\mathbf{c}^*$, $\mathbf{q}_2 = 1/2\mathbf{b}^* + 1/2\mathbf{c}^*$, and $\mathbf{q}_3 = -1/2(\mathbf{a}^* + \mathbf{b}^*) + 1/2\mathbf{c}^*$, respectively. Each CDW component has a different initial phase, that is, $\phi_1 = 0$, $\phi_2 = 2\pi/3$, and $\phi_3 = 4\pi/3$. As $H_{CDW} \equiv \mathbf{q}_1 \cdot (\mathbf{q}_2 \times \mathbf{q}_3) < 0$, this distribution is defined as left-handed chiral CDWs [Fig. 4(a)]. In addition, we suppose that there is a charged impurity at $(x, y, z) = (0, 0, 0)$. And then we assumed that the charge distribution for screening is simply induced by $\rho_{screen}(\mathbf{r}) = A/|r| \sum_{i=1,2,3} \cos(\mathbf{q}'_i \cdot \mathbf{r} + \phi'_i)$, where $A/|r|$ expresses a decay factor.²⁰ In Fig. 4, the bright red areas are charge density peaks formed by the intersection of wave planes in each xy plane. To focus on the position change of the charge density peak near the impurity, we show the density peak as a black solid circle and the impurity as a red cross. As the z position goes deeper, the peak position moves clockwise around the impurity in Fig. 4(a). When $\mathbf{q}'_i = \mathbf{q}_i$, $\phi'_i = \phi_i$, the peak position moves in the same way as the CDWs. In this case, the local chirality $H_{FO} \equiv \mathbf{q}'_1 \cdot (\mathbf{q}'_2 \times \mathbf{q}'_3) < 0$ so the FO is locally left-handed. This state describes the FOs without an inversion center caused by an atomic vacancy. Holes screen a negative charge, which is induced by a lack of Ti atoms as shown in Figs. 2(b) and 2(d). This is seen as a dark triangle. In contrast, when $\mathbf{q}'_i = -\mathbf{q}_i$, $\phi'_i = \phi_i$, The peak position moves anticlockwise [Fig. 4(b)].

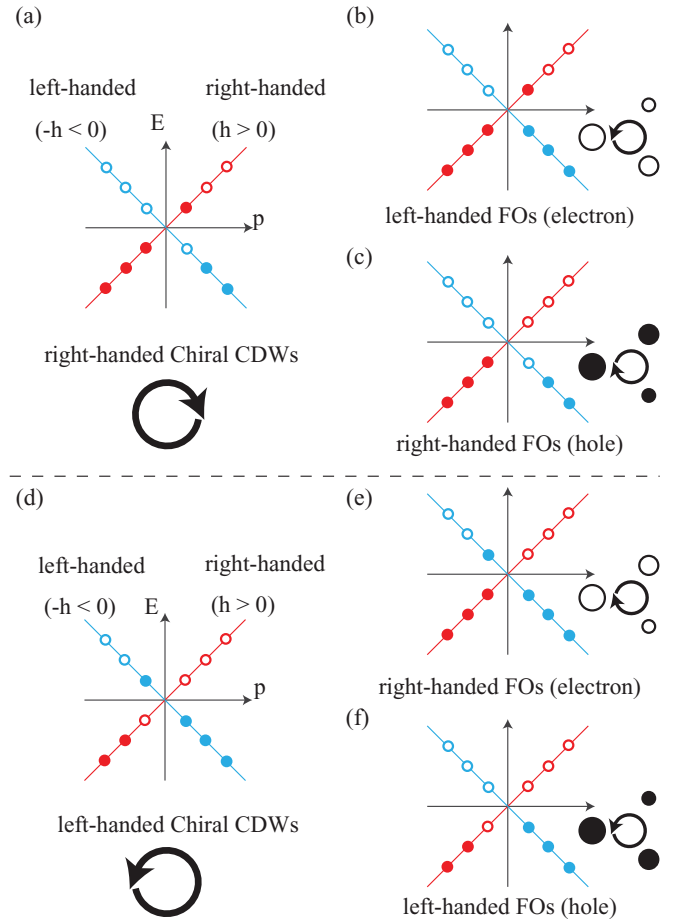


FIG. 5. (Color online) Schematic illustrations of a model of Dirac sea in CDWs. Each picture corresponds to (a) right-handed chiral CDWs, (b) left-handed bright FOs, (c) right-handed dark FOs, (d) left-handed chiral CDWs, (e) right-handed bright FOs, and (f) left-handed dark FOs. The filled red and blue circles are right-handed electron ($h > 0$) and left-handed electron ($-h < 0$), respectively. The opened red and blue circles are right-handed hole ($-h < 0$) and left-handed hole ($h > 0$), respectively.

$H_{FO} \equiv \mathbf{q}'_1 \cdot (\mathbf{q}'_2 \times \mathbf{q}'_3) > 0$. The FO is locally right-handed. This state describes the FOs with a mirror inversion caused by an intercalated atom. The electrons screen the positive charge induced by Ti intercalation into the van der Waals gap. This is seen as a bright triangle. The experimental results are consistent with the emergence of inverted chirality around FO from the underlying CDWs.

The relation between the FO and CDW can be understood from the particle picture (Fig. 5). Figure 5 shows the energy dispersion in momentum space. In Fig. 5, a branch denoted by a red line corresponds to a right-handed branch with positive helicity ($h > 0$), and that denoted by a blue line corresponds to a left-handed branch with negative helicity ($-h < 0$). Figure 5(a) shows the initial state of the right-handed chiral CDW. In this state, the difference of the number of the electron in the right-handed branch and the left-handed branch makes the right-handed chirality of CDWs. Then, adding an electron to the left-handed branch corresponds to Fig. 5(b). The removal of an electron from the right-handed branch corresponds to Fig. 5(c). Because removing an electron can be interpreted

to adding a hole to the system, these pictures represent the bright FOs and dark FOs, respectively. It reveals that adding and removing electrons decreases the helicity of the electron system in the same way. In terms of helicity, a bright FO and a dark FO are the same. With left-handed chiral CDWs, the chirality relation is the inverse of that in right-handed chiral CDWs [Figs. 5(d)–5(f)]. If there is only a single branch with a single helicity, the number of electrons simply correspond to number of helicities in the system. Thus, a single branch cannot explain why an increase in electrons causes a reduction in helicity. Therefore it is possible to understand our results by supposing that the CDW system has a Dirac-type dispersion curve with a set of right-handed and left-handed branches. This picture corresponds to the experimental results shown in Table I (insets in Fig. 5). The mechanism of the semiclassical picture of the quantum anomaly seems to work as if it were in the Dirac electron system.

For understanding chiral CDWs, another theoretical approach is proposed by introducing a concept of orbital

ordering.²⁴ The chiral-inverse FO may be understood by means of this concept, although it is not clear whether the addition of excess orbit of electron reduces a local helicity.

IV. CONCLUSION

In conclusion, we have discovered a chiral FO in chiral CDWs. We showed the relationship between chiral CDWs and chiral Friedel oscillations. From our analysis of chirality in an FO, we discovered that the CDW system consists of Dirac-type CDWs. Based on the fact that it can convert an electronic structure into a pattern in real space, an FO can be considered a “window” through which to see the ground state of an electronic system from real space to reciprocal space.

ACKNOWLEDGMENTS

We thank Y. H. Liu, K. Yamaya, T. Toshima, K. Inagaki, T. Matsuura, and H. Nobukane.

*tanda@eng.hokudai.ac.jp

¹T. D. Lee and C. N. Yang, *Phys. Rev.* **104**, 254 (1956).

²J. D. Watson and F. H. C. Crick, *Nature (London)* **171**, 737 (1953).

³P. M. Chaikin and T. C. Lubensky, *Principles of Condensed Matter Physics* (Cambridge, London, 1995).

⁴H. Nobukane, A. Tokuno, T. Matsuyama, and S. Tanda, *Phys. Rev. B* **83**, 144502 (2011).

⁵J. Ishioka, Y. H. Liu, K. Shimatake, T. Kurosawa, K. Ichimura, Y. Toda, M. Oda, and S. Tanda, *Phys. Rev. Lett.* **105**, 176401 (2010).

⁶J. M. Ziman, *Principles of the Theory of Solids* (Cambridge, London, 1965).

⁷F. Silly, M. Pivetta, M. Ternes, F. Patthey, J. P. Pelz, and W.-D. Schneider, *Phys. Rev. Lett.* **92**, 016101 (2004).

⁸O. Shiino, T. Endo, W. Yamaguchi, H. Sugawara, K. Kitazawa, and T. Hasegawa, *Appl. Phys. A* **92**, S175 (1998).

⁹F. J. DiSalvo, D. E. Moncton, and J. V. Waszczak, *Phys. Rev. B* **14**, 4321 (1976).

¹⁰K. C. Woo, F. C. Brown, W. L. McMillan, M. J. Scaffman, and M. P. Sears, *Phys. Rev. B* **14**, 3242 (1976).

¹¹I. Taguchi, M. Asai, Y. Watanabe, and M. Oka, *Physica B* **105**, 146 (1981).

¹²A. Zunger and A. J. Freeman, *Phys. Rev. B* **17**, 1839 (1978).

¹³E. Morosan, H. W. Zandbergen, B. S. Dennis, J. W. G. Bos, Y. Onose, T. Klimczuk, A. P. Ramirez, N. P. Ong, and R. J. Cava, *Nat. Phys.* **2**, 544 (2006).

¹⁴J. A. Wilson, *Solid State Commun.* **22**, 551 (1977).

¹⁵T. E. Kidd, T. Miller, M. Y. Chou, and T.-C. Chiang, *Phys. Rev. Lett.* **88**, 226402 (2002).

¹⁶G. Li, W. Z. Hu, D. Qian, D. Hsieh, M. Z. Hasan, E. Morosan, R. J. Cava, and N. L. Wang, *Phys. Rev. Lett.* **99**, 027404 (2007).

¹⁷K. Rossnagel, L. Kipp, and M. Skibowski, *Phys. Rev. B* **65**, 235101 (2002).

¹⁸C. G. Slough, B. Giambattista, A. Johnson, W. W. McNairy, C. Wang, and R. V. Coleman, *Phys. Rev. B* **37**, 6571 (1988).

¹⁹R. V. Coleman, B. Giambattista, P. K. Hansma, A. Johnson, W. W. McNairy, and C. G. Slough, *Adv. Phys.* **37**, 559 (1988).

²⁰I. Tutto and A. Zawadowski, *Phys. Rev. B* **32**, 2449 (1985).

²¹S. E. Barnes and A. Zawadowski, *Phys. Rev. Lett.* **51**, 1003 (1983).

²²We have performed the same experiments on 1T-TiSe₂ at 300 K and found no CDWs and chiral FOs. From the point of view that high-T_c CDWs may have incoherent CDWs even above T_c, FOs can be interpreted to local CDWs. As the temperature decreases, entire CDWs overlap FOs with the opposite chirality. As for local CDWs, see G. P. E. M. Van Bakel and J. T. M. De Hosson, *Phys. Rev. B* **46**, 2001 (1992).

²³A. S. Razinkin, A. N. Enyashin, T. V. Kuznetsova, A. N. Titov, M. V. Kuznetsov, and A. L. Ivanovskii, *J. Str. Chem.* **51**, 737 (2010).

²⁴J. van Wezel (Private communication).